

A NEW 2.5D DISTRIBUTED SPICE MODEL OF SOLAR CELLS

S. E. Foss*, B. R. Olaisen, E. S. Marstein and A. Holt
Section for Renewable Energy, Institute for Energy Technology
P.O. Box 40, NO-2027 Kjeller, Norway
Telephone: +47 63806104, Fax: +47 63812905, *sean.erik.foss@ife.no

ABSTRACT: A general distributed circuit model of a solar cell has been developed for simulating a range of conditions. The model is based on standard equivalent circuits representing one- or two-diode models of a solar cell. In the new model, the full sized solar cell is modeled as a distributed, interconnected network of such equivalent circuits. Interconnecting resistors represent emitter series resistance, contact resistance, resistance in the metal grid and shunting resistance. This approach enables a realistic model of a solar cell with inhomogeneities as all resistor and diode parameters may be set separately for each element. As examples of usage three different cases were investigated. In one case the effect of uneven sheet resistivity is studied. The second case looks at the effect of broken metal fingers, and the third case looks at the effect of local shunts. Results using the model are obtained by SPICE simulations. This enables a fast calculation of current and potential distribution in the model circuit. Current and potential maps from a model solar cell consisting of several thousand elements may be calculated within seconds
Keywords: Silicon, Modeling, Simulation, Distributed, Inhomogeneous

1 INTRODUCTION

As commercial solar cells are steadily increasing in surface area while at the same time the margins of error are decreasing for an efficient cell, a good understanding of the effect of different cell parameter inhomogeneities is imperative. Mapping techniques for characterizing solar cells are more frequently used. In order to fully benefit from such techniques, an increased understanding of the quantitative consequences of spatial inhomogeneities on solar cell performance is needed. Coupling such spatially resolved data to a distributed model, as presented here, may be of great help in understanding and optimizing the cell processing and design.

Several methods have been suggested in the past for optimizing separate parts of a solar cell, e.g. the front contact grid [1]. These usually take into account only a subset of the effects present in a cell. To improve on this it is possible to look at the combination of these different components and the effect of the physical distribution of the cell in a calculation. Distributed models have been studied earlier [2-6], however, the focus has been on different aspects.

2 THE MODEL

2.1 A distributed solar cell model

One way of looking at several of these factors simultaneously is to expand on the well-known one- and two-diode models of the single junction solar cell [1] and divide a typical cell into several smaller cell elements, each containing a diode model. Figure 1 shows a schematic of the model. A standard n^+pp^+ solar cell structure is the basis for the model. By using simple circuit elements such as resistors and diodes, a spatially as well as physically detailed model of the solar cell may be built and simulated on a computer. This approach will help quantize the effect inhomogeneities have on the cell performance as well as take into account several distinct distributed resistive loss factors. The lumped one- or two-diode model incorporates much of the distributed device physics in very few parameters and is therefore not suited for describing most real cases.

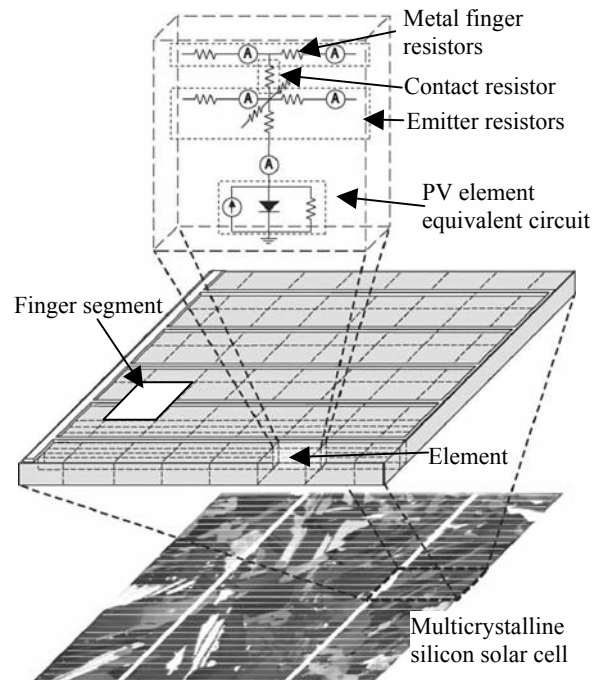


Figure 1: The principle of the presented model. The cutout schematic above the image of a solar cell shows the model geometry used. Each finger segment, as shown, consists of several elements. Each element consists of an equivalent circuit shown in the diagram at the top. All elements are connected by resistors to each nearest neighbor.

A one- or two-diode lumped model takes into account many of the loss-mechanisms observed in a solar cell. In Fig. 2 a diagram of the lumped model is shown. It includes a current source representing the photo induced current generation in the volume of each element and one or two diodes in parallel with ideality factors and saturation currents corresponding to the recombination mechanisms they represent. In the present model, two-diode models are used with diode ideality factors of 1

and 2 representing recombination in the neutral region and recombination in the depletion region respectively.

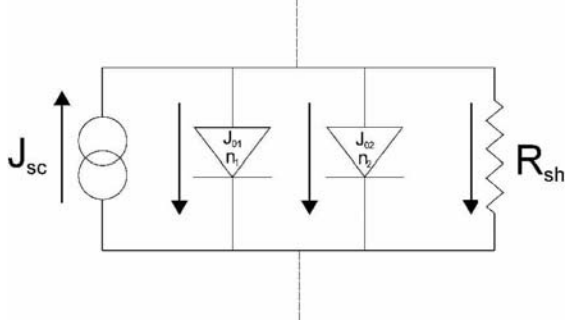


Figure 2: The equivalent circuit of a PV element used in the present model. J_{sc} is the generated current in the volume of the element, J_{01} and J_{02} are the saturation currents for diode 1 and 2, and n_1 and n_2 are the ideality factors for each diode. R_{sh} is the shunt resistance. The arrows indicate the direction of the current during normal operation of the element.

Each of the distributed model elements contain a single- or two-diode equivalent circuit with a shunt resistor in parallel (PV element in Fig. 1), a base resistor connecting the PV element to the backside contact or ground representing the bulk resistivity, emitter resistors connecting to other elements representing series resistance in the emitter and contact resistors between emitter and contact fingers, if applicable, representing contact resistance.

The fingers are modeled as a series of single resistors while the busbar is considered to be at equipotential and not modeled with resistors. This is mainly to avoid any ambiguity when comparing to measured IV curves as to where the busbar in the measurement setup has been contacted, hence the busbar resistance will not be a factor in the present model. Some of the resistor values used in the model are defined in Table 1.

The elements represent the dimension along the axis normal to the solar cell surface, hence the model is not a true 3-dimensional model – one dimension is not free. These elements are connected together to form a network of resistors and diodes. The network is set up so that it contains the physical dimensions and topology of the real solar cell.

Table 1: Definition of some of the resistor values used in each element in the model. ρ_{sq} is the emitter sheet resistivity, ρ_f is the specific resistivity of the finger metal and ρ_c is the contact resistivity. l_s is the segment width and l_e is the element breadth. w_f and h_f are the finger width and height respectively.

Emitter resistor value - element to element, same segment	$R_{ee} = \rho_{sq} \cdot \frac{l_e}{l_s}$
Emitter resistor value – between segments	$R_{es} = \rho_{sq} \cdot \frac{l_s}{l_e}$
Metal finger resistor value	$R_f = \rho_f \cdot \frac{l_s}{w_f \cdot h_f}$
Contact resistor value	$R_c = \frac{\rho_c}{l_s \cdot \frac{1}{2} w_f}$

2.2 Implementing the model

The resistor and diode network is built semi-automatically with a Python script [7]. The input parameters are the topography of the model cell, e.g. size and the number of fingers, and the physical parameters, e.g. sheet resistivity and contact resistivity, as well as model parameters such as element size and diode model. As each component in each element is controllable through this script, measured spatially dependent data may be used as input. This may be sheet resistivity maps from an actual cell or spatially dependent lifetimes such as in a multicrystalline cell. Spatially varying lifetimes may be represented as spatially dependent diode saturation currents [4]. However, the measured data may not be sampled on the same grid as the model, hence interpolation of the data may be necessary.

An efficient calculation of the current and potential distribution in the resistor and diode network as a function of externally applied voltages is enabled by the use of the SPICE circuit simulator. A typical model consists of 50000 elements. A simulation run for this model for one externally applied voltage value is done in about 12 seconds on a 2 GHz PC. However, the computation time does not scale linearly with the number of elements. The computation time may be stated as βN^α where N is the number of elements and β is a factor and α is between 2 and 3 as has been reported by B. Galiana [3] for a similar model.

2.3 Input parameters

A baseline model is made by using values for the resistors and diodes that are calculated from parameters obtained by IV measurement of a standard multicrystalline solar cell. The IV curve is shown in Fig. 3. Fitting of data to a single- and two-diode model using IVfit from ECN [8] is used to obtain shunt resistance, short-circuit current and saturation currents, while emitter sheet resistance is obtained either by four-point probe measurement or sheet resistance mapping with a SemiLab WT2000 instrument. Contact resistance is obtained from the literature [9]. The base resistor (not shown in Fig. 1) is calculated based on the nominal bulk resistivity used for standard multicrystalline solar cells.

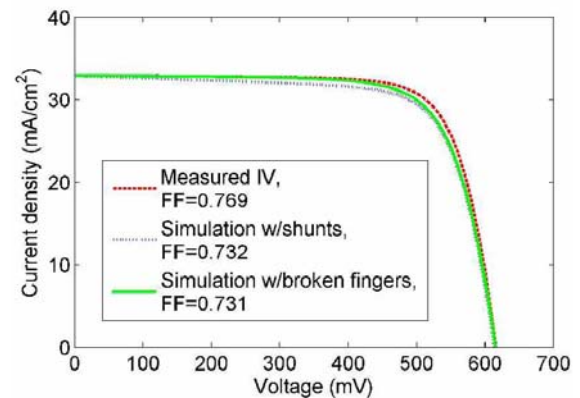


Figure 3: IV curves of an actual multicrystalline solar cell (red - dashed), a simulated model with point shunts (blue - dotted), and a simulated model with broken fingers (green - whole). The simulated models are described in the text.

The network typically consists of 10 segments along the fingers on each side of the busbar, each roughly 3 mm long. Each segment is typically divided into 5 elements on each side of the finger, each element about 250 μm wide. The model has two busbars and 48 fingers as well as a contacting line along the rim of the cell. There are no elements beneath the fingers or busbars, hence there is 100 % shading at these positions. In a further development of the model it would be natural to include elements also here, but with a reduced current generation according to the level of shading so as to enable the current paths that are physically present beneath the metal lines. Elements on either side of a finger are connected through a contact resistor. Edge-shunting has not been included in this model.

Figure 4 shows a map of a typical multicrystalline solar cell emitter. This has been used in some of the simulations to show the effect of real inhomogeneous emitter sheet resistivity. As seen in Fig. 4 there are slight inhomogeneities across the whole cell, in addition there is one area with a significantly larger sheet resistivity. The mean resistivity is 34 Ω/\square with a standard deviation of 3 Ω/\square .

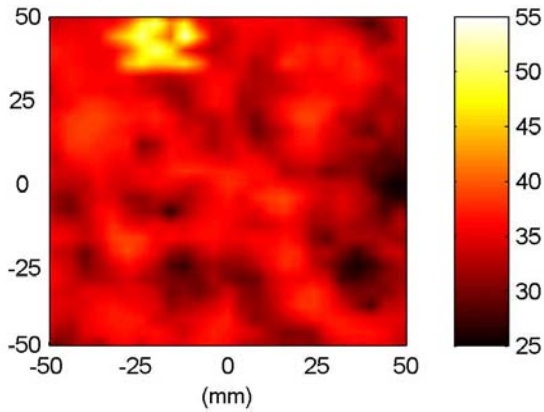


Figure 4: Map of measured sheet resistivity of the emitter of an actual multicrystalline solar cell. These values are used in the simulation of the distributed solar cell model. The color bar on the right shows the range of sheet resistivities measured in Ω/\square .

2.4 Output and data analysis

IV curves from a model simulation are obtained by extracting the resulting current between the busbar and cell backside (ground) in the external circuit as a function of applied external voltage, analogous to what is done in experiments. IVfit has also been used here to obtain parameters so a comparison may be made between the IV curve obtained from the actual solar cell mentioned earlier and an IV curve from the distributed model.

3 RESULTS

To verify that the modeling and simulation give reasonable results, a series of models of simple, idealized cells were constructed and simulated. These models were constructed to resemble the baseline model and real cell described earlier, only varying cell parameters such as ρ_{sq} , ρ_f , and ρ_c .

3.1 The effect of finger resistivity

Figures 5 and 6 shows the emitter potential distribution close to the maximum power point (MPP) of 0.5 V for two models, both with $\rho_{sq}=38 \Omega/\square$, $R_{sh}=10.0 \Omega$, and $\rho_c=1.0 \cdot 10^{-2} \Omega \cdot \text{cm}^2$, but with differing finger metal resistivities of $1.5 \cdot 10^{-5} \Omega \cdot \text{cm}$ and $1.0 \cdot 10^{-6} \Omega \cdot \text{cm}$ respectively. Note that the scale of the color bar is the same for Figs. 5 to 8. One may see that in the case with the high finger metal resistivity the emitter potential range is larger than in the low resistivity. The potential gradient along the fingers is higher in the high resistivity case. This indicates that more current moves in the emitter. Fill factors obtained by IVfit for these two cases are 0.77 for the low resistivity case and 0.75 in the high resistivity case. The fitted series resistances were $2.9 \cdot 10^{-3} \Omega$ and $5.6 \cdot 10^{-3} \Omega$ respectively.

The IV curve obtained from a real multicrystalline solar cell with an efficiency of 15.4 % is shown in Fig. 3. The IV curve from a simulation of a distributed model using parameters obtained from fitting the real IV curve and other parameters, as mentioned earlier, shows only small deviations. The parameters from the fit are shown in Table 2. As the R_{se} parameter from the measurement comprises several factors contributing to the series resistance, the values chosen for these factors in the model cell may not correlate exactly to the real cell. Best guess values from other measurements are therefore used. Parameters obtained from a fit of the IV data obtained from the simulation of one such model is shown in Table 2 as well. In this case realistic emitter sheet resistivity data was used as well as a contact resistivity, ρ_c , of $1.0 \cdot 10^{-3} \Omega \cdot \text{cm}^2$, and finger metal resistivity, ρ_f , of $1.5 \cdot 10^{-5} \Omega \cdot \text{cm}$.

Table 2: Obtained parameters from the IV curve of a real multicrystalline solar cell using IVfit and parameters from a simulated model based on parameters from the real cell. The IV curve was measured under standard conditions: 1 sun, 1.5 AM, 25 °C.

Parameter	Real cell	Model cell (real parameters)
J_{sc}	32.99 mA/cm ²	32.97 mA/cm ²
J_{01}	$1.2 \cdot 10^{-9}$ mA/cm ²	$9.5 \cdot 10^{-10}$ mA/cm ²
J_{02}	$4.4 \cdot 10^{-5}$ mA/cm ²	$4.9 \cdot 10^{-5}$ mA/cm ²
R_{sh}	10.0 Ω	10.0 Ω
R_{se}	$3.5 \cdot 10^{-3}$ Ω	$4.3 \cdot 10^{-3}$ Ω
FF	0.769	0.760
η	15.4 %	15.4 %
V_{oc}	611 mV	616 mV

3.2 The effect of local shunting

Figure 7 shows the potential distribution in a case where a model including five elements where R_{sh} is set to $1.0 \cdot 10^{-6} \Omega$ has been simulated. This could represent a solar cell where the finger metal has been locally fired through the pn-junction. From the figure the shunted elements are clearly visible as sharp dips in the potential, however, it generally seems as if the potential distribution is not much disturbed except for at the shunt between the busbars. This is also reflected in the fitted parameters. The IV curve of this model is shown in Fig. 3, and a significant but small shunt effect is visible as well as a small decrease in fill factor. The R_{sh} in this case

is 2.2Ω compared to 10.0Ω in the baseline and real cases.

3.3 The effect of broken fingers

Another inhomogeneous factor observed in cell processing is broken metal fingers. Depending on the emitter sheet resistivity, contact resistivity and finger resistivity the effect of broken fingers will vary. Shown in Fig. 8 is the potential distribution of a model cell at MPP. The cell parameters are the same as for the model presented in Fig. 7, but a number of broken fingers are included. This is realized by removing the finger resistor between two segments (see Fig. 1). In this model, three areas have been partly isolated. In addition five finger resistors have been randomly removed. These breaks in the finger result in locally, as well as distributed, higher potentials due to the increased current in the emitter circumventing the breaks. A maximum potential of 0.61 V for the large isolated area is observed. This is 0.11 V larger than the busbar voltage and the MPP of each element, hence parts of the cell operate relatively far away from the total cell MPP. The IV curve from this model is also shown in Fig. 3. Again, only a small effect is seen, mainly in the fill factor.

These simulations indicate the robustness of a typical solar cell. The relatively high resistance in the emitter isolates local faults, and as long as a fairly large part of the cell is intact, the efficiency is maintained.

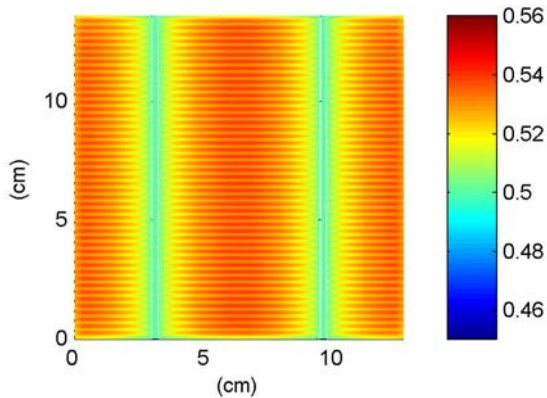


Figure 5: Emitter voltage distribution for a model cell using a homogeneous emitter with a sheet resistivity of $38 \Omega/\square$, $R_{sh}=10.0 \Omega$, $\rho_f=1.5 \cdot 10^{-5} \Omega\text{-cm}$, and $\rho_c=1.0 \cdot 10^{-2} \Omega\text{-cm}^2$. External voltage (between busbar and backside) is 0.5 V , close to the MPP.

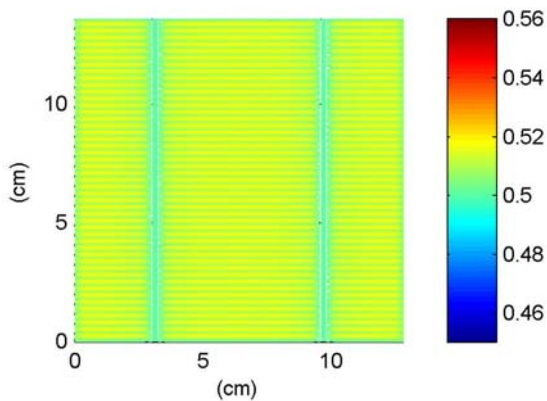


Figure 6: Emitter voltage distribution for a model cell using a homogeneous emitter of $38 \Omega/\square$, $R_{sh}=10.0 \Omega$,

$\rho_f=1.0 \cdot 10^{-6} \Omega\text{-cm}$, and $\rho_c=1.0 \cdot 10^{-2} \Omega\text{-cm}^2$. External voltage is the same as in the case in Fig. 5.

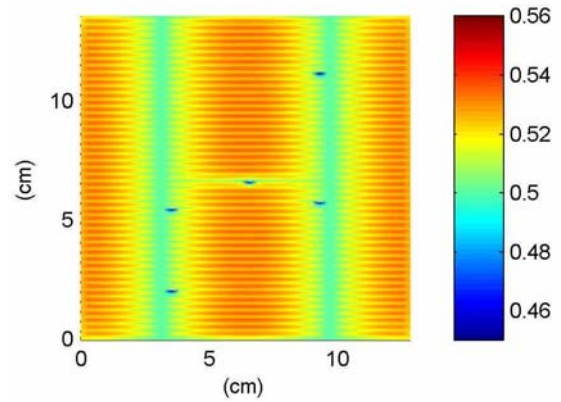


Figure 7: Emitter voltage distribution for a model with five local shunts. The R_{sh} for each shunted element is set to $1.0 \cdot 10^{-6} \Omega$. In this case $\rho_{sq}=38 \Omega/\square$, $R_{sh}=10.0 \Omega$ for the other elements, $\rho_f=1.5 \cdot 10^{-5} \Omega\text{-cm}$, and $\rho_c=1.0 \cdot 10^{-3} \Omega\text{-cm}^2$. External voltage is the same as in the case in Fig. 5.

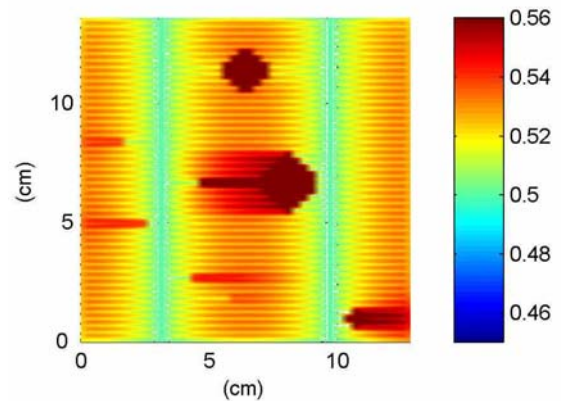


Figure 8: Emitter voltage distribution for a model with several breaks in the fingers. Three areas are isolated by cutting the metal fingers around the area which results in elevated voltages. The model parameters are the same as for the results shown in Fig. 7. External voltage is the same as in the case in Fig. 5.

4 CONCLUSION

A modeling and simulation framework based on SPICE circuit simulation has been developed and verified to give reasonable results. A model cell consists of multiple elements, each containing a PV equivalent circuit and resistors representing the different series resistance factors. The framework facilitates the use of inhomogeneous solar cell parameters, making it possible to more closely model realistic solar cells.

A few different modeling cases have been shown to give the expected results. Several other effects may be modeled as well, e.g. the effect of varying lifetime in a multicrystalline cell, the effect of varying reflectivity or incident light intensity as well as uneven contact firing. Work is currently underway to investigate these and other effects using the presented framework.

ACKNOWLEDGEMENTS

This work has been partly funded by Nordic Energy Research through the scientific project “Solar Electricity, from Materials to Systems Integration” (Nordic PV).

REFERENCES

- [1] M. A. Green, *Silicon Solar Cells – Operating Principles, Technology and System Applications*, Prentice-Hall, Englewood, Cliffs, NJ, 1982
- [2] P. P. Altermatt, G. Heiser, A. G. Aberle, A. Wang, J. Zhao, S. J. Robinson, S. Bowden, and M. A. Green, *Progr. Photovolt.* 4 (1996) 399
- [3] B. Galiana, C. Algora, I. Rey-Stolle, and I. G. Vara, *IEEE Trans. Electron. Devices* 52 (2005) 2552
- [4] U. Rau, P. O. Grabitz, and J. H. Werner, *Appl. Phys. Lett.* 85 (2004) 6010
- [5] E. T. Franklin and J. S. Coventry, *Proceedings 40th Annual Conference for the Australian New Zealand Solar Energy Society* (2002)
- [6] K. Araki and M. Yamaguchi, *Solar Energy Materials & Solar Cells* 75 (2003) 467
- [7] <http://www.python.org/>
- [8] A. R. Burgers, J. A. Eikelboom, A. Schonecker, and W. C. Sinke, *Proceedings 25th IEEE Photovoltaic Specialists Conference* (1996), (<http://www.ecn.nl/zon/products/ivfit/index.en.html>)
- [9] D. K. Schroder and D. L. Meier, *IEEE Trans. Electron. Devices* ED-31 (1984) 637